Imaging One-Dimensional and Two-Dimensional Planar Photodiode Detectors Fabricated by Ion Milling Molecular Beam Epitaxy CdHgTe

R. HAAKENAASEN,[1,3] H. STEEN,[1] E. SELVIG,[1] T. LORENTZEN,[1] A.D. VAN RHEENEN,[1] L. TROSDAHL-IVERSEN,[1] H. SYVERSEN,[1] D. HALL,[2] and N. GORDON[2]

1.—Norwegian Defense Research Establishment, P.O. Box 25, 2027 Kjeller, Norway. 2.—QinetiQ, St. Andrews Road, Malvern, Worcestershire, WR14 3PS, United Kingdom. 3.—E-mail: randi.haakenaasen@ffi.no

Imaging one-dimensional (1-D) and two-dimensional (2-D) arrays of mid-wavelength infrared (MWIR) and long-wavelength infrared (LWIR) planar photodiodes were fabricated by ion milling of vacancy-doped molecular beam epitaxy $Cd_xHg_{1-x}Te$ layers. Sixty-four-element 1-D arrays of $26 \times 26\ \mu m^2$ or $26 \times 56\ \mu m^2$ diodes were processed. Zero-bias resistance-area values (R_0A) at 77 K of $4 \times 10^6\ \Omega cm^2$ at cutoff wavelength $\lambda_{CO} = 4.5\ \mu m$ were measured, as well as high quantum efficiencies. To avoid creating a leakage current during ball bonding to the 1-D array diodes, a ZnS layer was deposited on top of the CdTe passivation layer, as well as extra electroplated Au on the bonding pads. The best measured noise equivalent temperature difference (NETD) on a LWIR array was 8 mK, with a median of 14 mK for the 42 operable diodes. The best measured NETD on a MWIR array was 18 mK. Two-D arrays showed reasonably good uniformity of R_0A and zero-bias current (I_0) values. The first 64×64 element 2-D array of $16 \times 16\ \mu m^2$ MWIR diodes has been hybridized to read-out electronics and gave median NETD of 60 mK.

Key words: CdHgTe, HgCdTe, CdZnTe, long-wavelength infrared (LWIR), mid-wavelength infrared (MWIR), ion milling, molecular beam epitaxy, n-on-p diodes, photodiodes, planar diodes, linear array, two-dimensional (2-D) array, IR detector

INTRODUCTION

There are many methods for making pn junctions in $Cd_xHg_{1-x}Te$ (CMT). These include ion implantation, in-situ growth of the dopants, and dry etching. Although fabricating high-quality diodes by any of these techniques is challenging, dry etching such as ion milling or reactive ion etching (RIE) is a relatively simple technique that has been studied in more detail recently.[1]

Ion milling of p-type vacancy-doped CMT releases Hg atoms that diffuse into the sample and fill in Hg vacancies, thereby revealing a background n-type carrier concentration and creating a pn junction.[1–6] Experiments show that in thin layers (<10 μm), the junction depth is linear with the milling time and milling current, and inversely proportional to the vacancy concentration,[2,4,5] while for longer milling times, the conversion depth is limited by a diffusion-like process and increases as the square root of time.[3,6] These results are probably not contradictory, and can be explained in an extended diffusion model.[7]

Diodes can be fabricated in a planar process, in which the pn junction at the surface of the CMT is created under the passivation layer and is therefore never exposed to air. We have reported linear arrays of high-quality diodes fabricated in such a process earlier.[8] In this paper, we present results from our first imaging one-dimensional (1-D) and

(Received October 7, 2004; accepted December 10, 2004)

two-dimensional (2-D) arrays, and we show that ion milling can be used to make arrays with good uniformity, high dynamic resistance and spectral response values, and low noise equivalent temperature difference (NETD) values.

The RIE on CMT also converts p-type material, with either vacancy- or extrinsic doping, to n-type, and small mid-wavelength infrared (MWIR) 2-D arrays with good device characteristics and long-wavelength infrared (LWIR) test diodes have been reported recently.[9–11]

EXPERIMENT

The 9–10 μm thick CMT layers with composition $x \sim 0.2$ and $x \sim 0.3$ were grown by molecular beam epitaxy (MBE) on (211)B oriented CdZnTe (CZT) substrates at a substrate temperature of ~195°C.[12] The background n-type doping carrier concentration was $3–5 \times 10^{15}$ cm^{-3}. In most of the layers, the Cd content x was varied by 0.02 over the thickness of the layer, with decreasing x-value toward the top of the layer. The gradient profiles are described in more detail in Ref. 8. The gradient creates a pseudo-electric field, which should help the electrons to move toward the pn junction and thereby be collected more efficiently, and previous results indicate higher and more uniform RA values on such layers. The 0.5 μm thick CdTe (CT) passivation layers were grown in situ at a substrate temperature of 250°C. The passivation layer is in reality a high x-value CMT layer, as there was still a Hg atmosphere in the growth chamber during this growth. The passivated layers were annealed in vacuum at 250°C for 24 h to give p-type vacancy doping with carrier concentrations at 77 K in the range $(N_a - N_d)_{77} \sim 1 - 4.5 \times 10^{16}$ cm^{-3} and hole mobility ~300 cm^2/Vs for MWIR and ~600 cm^2/Vs for LWIR layers.

The 0.3 μm ZnS was then thermally evaporated onto some samples selected for 1-D arrays. ZnS is a much better insulator than CdTe, and this is important for the 1-D arrays, which have long lead-out wires and bonding pads deposited on top of the passivation. Large lead-out Au areas directly on top of the CT passivation were in some cases clearly seen to increase the leakage current and thereby decrease the R_0A values of the diodes. The effect of ball bonding was much worse, and often resulted in small or significant reduction in R_0A up to the point where a diode must be defined as inoperable. ZnS was deposited either on top of a photoresist mask which covered the diode areas, or on a larger rectangular mask which covered all the diodes and the area immediately surrounding them. In this way, we could use our regular method for diode processing (without etching ZnS), but have extra insulation under the bonding pads and most of the lead-out wires.

ZnS was not necessary for the 2-D array samples, as these were flip-chip bonded and therefore had no lead-out wires deposited on top of the passivation layer.

Sixty-four element linear arrays or 64 × 64 element 2-D arrays were fabricated by ion milling. The dimensions and some characteristics of the arrays presented here are listed in Table I. In addition, test samples with 2-D arrays of different size diodes were fabricated. These had two arrays with 64 × 64, 30 μm pitch, 16 × 16 μm^2 diodes and one array with 34 × 78, 55 μm pitch, 37 × 37 μm^2 diodes. On one of the 64 × 64 arrays, and on a part of the 34 × 78 array, some diodes were left out in the mask and Cr/Au bonding pads were sputtered on top of the CT passivation instead. There were such bonding pads for 120 of the small diodes and 40 of the large diodes, and these were used for test measurements.

A wet etch was used to remove the CT passivation layer from the diode areas. Then ion milling was performed immediately without removing the photoresist wet-etch mask from the sample. (In a few samples, a new photoresist mask with slightly larger opening areas was deposited after wet etch but before ion milling.) The milling current density was $I_{IM} = 0.54$ mA/cm^2 and the milling time t = 17–21 sec, which resulted in a pn junction at depth ~3.5–4 μm with lateral extension ~1.75–2 μm under the CT passivation.[4,5] A Kaufman ion gun was used, and the accelerated ions (700 eV) were incident at a 45° angle with the surface, while the sample was rotated and cooled during milling. Sputtering of Cr/Au contacts started a few seconds after the milling. Then the p-type contact was made and 0.45 μm thick Au lead-out wires and bonding pads were sputtered on top of the passivation.

To further decrease the chances of destroying diodes during ball bonding, a 1 μm thick Au layer was electroplated on top of the sputtered Au 1-D array bonding pads. This made a soft enough "cushion" for the bonding ball that RA curves did not usually degrade after bonding.

Current-voltage (IV) and spectral response measurements were performed at 77 K in a probe station, in a cryostat, or in a dewar. In the probe station, the arrays were front illuminated by the background

Table I. Overview of the Diode Arrays

Sample	λ_{CO} (μm)	Diode Size (μm × μm)	Pitch (μm)	Number of Diodes	NETD Best/ Median (mK)
484-2	4.5	26 × 26	50	64	—
492-4	5.5	26 × 26	50	64	18/—
577-5	8.4	26 × 56	50	64	8/14
524-5	5.3	16 × 16	30	64 × 64	26/60

radiation in the room, while in the cryostat, the measurements were made in the dark. For imaging, the 1-D arrays were ball bonded to a sample holder in a dewar in the back-illuminated configuration. The dewar had a Ge window with antireflective (AR) coatings on both sides. Read-out electronics consisted of a conventional current-to-voltage converter, and images were taken with a simple setup consisting of a rotating mirror, a ZnS lens, and a digital data sampling system. The NETD was calculated from the response from two blackbody sources differing by 10 K. Indium bumps were deposited on the diodes in several 2-D arrays. Only one 2-D array has been hybridized and mounted for imaging so far.

RESULTS

1-D Arrays

High zero-bias resistance-area values R_0A (in excess of 1×10^7 Ωcm^2 for cutoff wavelength $\lambda_{CO} \sim 4.5$ µm and 3×10^2 Ωcm^2 for $\lambda_{CO} \sim 9$ µm at 77 K) and quantum efficiencies have been reported earlier[8] for test diodes or smaller arrays of 32 elements.

Figure 1 shows current (I) and differential resistance times area (RA) versus bias voltage at 77 K for a 64-element 1-D array with $\lambda_{CO} = 4.5$ µm (sample 484-2). The Au lead-out wires were deposited directly on top of the CT passivation in this sample. The measurements were made in a probe station and the diodes were therefore front illuminated by the background radiation in the room. As can be seen from the figure, the uniformity of the array is good. The average R_0A value for 61 of the diodes is 1.4×10^4 Ωcm^2, and for the same 61 diodes, the negative of the zero-bias current $(-I_0) = 3.3$ nA $\pm$ 0.6 nA. The leakage current is small out to a large (>0.5 V) reverse bias.

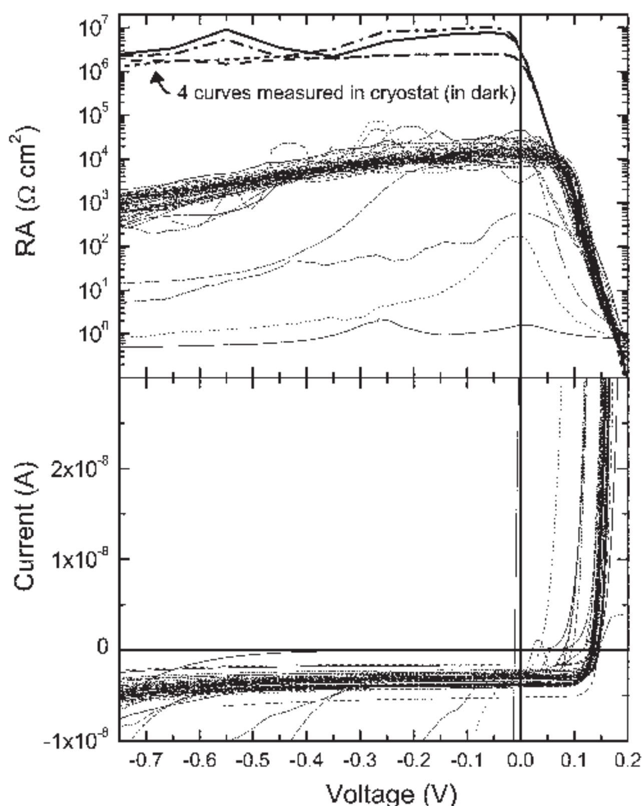

Fig. 1. RA-V and IV curves measured in the probe station at 77 K for a 64-element 26 × 26 µm² 1-D array with λ_{CO} = 4.5 µm (Sample 484–2). The four highest curves in the top plot are the RA-V curves for four of the diodes measured in a dark cryostat at 77 K.

Overlaid on the top plot are the RA curves for four of these diodes measured in a cryostat in the dark at 77 K. In the dark, the R_0A and $R_{max}A$ values are 1.5–4 $\times 10^6$ Ωcm^2 and 2.5–10 $\times 10^6$ Ωcm^2, respectively. Although this is a small diode selection, we have no reason to believe that the other diodes would behave differently, especially since the probe measurements suggest good uniformity and a small leakage current out to large reverse bias. Apparently, the large background flux during the probe measurements has a strong effect on the R_0A values. It has been suggested[13] that such large fluxes could reduce the R_0A value through a bias-induced modulation of the collection efficiency, analogous to the Early effect in bipolar transistors. A quick estimation of this effect for our diodes does not preclude such an explanation. Previous measurements on this sample (Ref. 8) show that it does also have a bias-dependent gain of the photogenerated carriers and that this accounts for much of the increase in current out to reverse bias of 1.5 V. This may also contribute to the increase in RA values with decreasing photocurrent.

Spectral response measurements at 77 K of seven circular diodes of four different sizes from sample 484-1 (same growth layer as the one in Fig. 1) are shown in Fig. 2. The diodes are measured in the back-illuminated configuration. The apparent quantum efficiency (the value calculated using the ion-milled area for the diodes, without correction for lateral collection) is quite flat with λ, and fits of the square root of the apparent quantum efficiency versus inverse diode radius give a lateral optical collection length $L_{opt} \sim 24$ µm and a bulk quantum efficiency $\eta \sim 0.9$. Insufficient measurements at

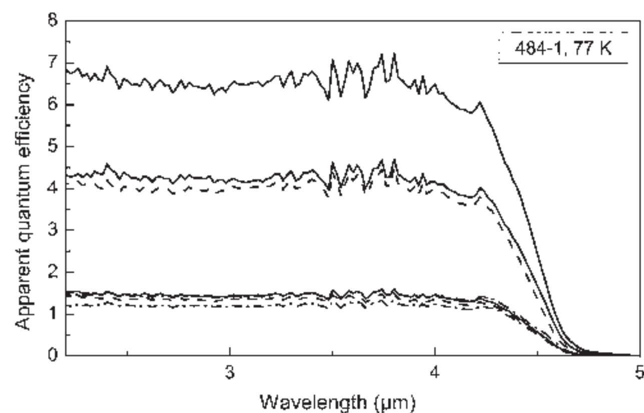

Fig. 2. Measured apparent quantum efficiency versus wavelength at 77 K for seven circular diodes of four different sizes from the same growth layer (but different sample) as the one in Fig. 1.

different diode areas lead to uncertainty and a too high η (should not be more than ~0.7 for a sample without AR coating). A more detailed analysis of spectral response measurements from many samples will be published later.

Unfortunately, most of the diodes in the array on sample 484-2 were degraded during ball bonding to read-out electronics, so imaging was not attempted.

The alternative approach with a thermally evaporated layer of ZnS on top of the CdTe passivation was then investigated. A 64-element LWIR linear array was processed on sample 577-5, which had λ_{CO} = 8.4 μm. Both the ZnS passivation layer and the extra electroplated gold on the bonding pads were deposited. Unfortunately, one area of the sample gave poor IV characteristics before bonding, and there was a problem with some completely or partially missing lead-out wires/bonding pads. Also, a few diodes had been previously bonded for spectral response test measurements. However, of the 45 diodes that had reasonable RA ($R_0A \sim 20$, $R_{max}A \sim$ 40–70 at 77 K) and intact bonding, 42 were defined as operable according to NETD measurements. These gave NETD values ranging from 8 mK to 51 mK, with a median of 14 mK, as shown in Fig. 3. The field of view (FOV) was 22°, and the array was backside illuminated and at temperature 77 K. A 77 K image taken with this array is shown in Fig. 4.

In order to estimate an experimental limit for NETD, the diodes were irradiated by a black body that was varied between 22°C and 40°C and that covered the entire FOV. From measurements of the photocurrent (I_{ph}), using a simple current-to-voltage converter, the responsivity R (in A/K) was extracted. Also, the shot noise in the currents was calculated from the photocurrents, $S_I = 2qI_{ph}$, where q is the electron charge. The experimental NETD limit for the diodes was then calculated from NETD(limit) = $(1/R)\sqrt{(S_I \times BW)}$, where the bandwidth BW of the current-to-voltage converter was 25 kHz. If no other noise sources were present, we estimate the experimental NETD limit for these diodes to be 7 mK.

A 64-element linear array was processed in the same way on a MWIR sample (492-14), which had λ_{CO} = 5.5 μm, quantum efficiency ~ 0.8, and L_{opt} ~12 μm. The best measured NETD on this array was 18 mK.

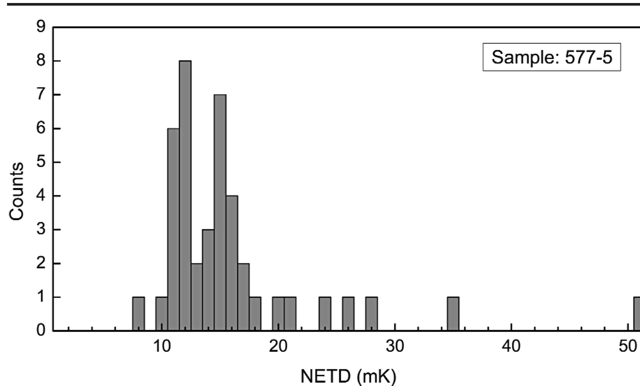

Fig. 3. NETD histogram of the 42 operable diodes on a 64-element 26 × 56 μm² diode LWIR linear array with λ_{CO} = 8.4 μm. The FOV was 22° and the array temperature was 77 K.

2-D Arrays

Test samples with the 2-D arrays of different size diodes were fabricated. Figure 5 shows the R_0A values measured at 77 K in the probe station from all 120 16 × 16 μm² test diodes (called small diodes) and 40 37 × 37 μm² test diodes (called large diodes) on such a sample (524-2) with λ_{CO} = 5.3 μm. The diodes are sorted by increasing R_0A value. Again, the values measured in the probe station are not the highest RA values obtainable (which would indicate diode quality), but they tell us that the diode RA values are at least as good as these values. In addition, they can give a good indication of the uniformity of the diodes. Figure 6 shows $-I_0/A$ values for the same diodes sorted by $-I_0/A$ values (five of the diodes with the lowest R_0A values in Fig. 5 had negative $-I_0/A$ and are not included in Fig. 6). The arrays are reasonably uniform, and investigations of many arrays show that the processing is spatially uniform over a 5 × 5 mm² area. The corresponding I_0R_0 values in units of kT/q are shown in Fig. 7 (sorted by I_0R_0 values and also missing the five first diodes in Fig. 5). Here k is the Boltzmann constant and T is temperature. The condition for background-limited performance is often written as $R_0 >> kT/(q\ I_{ph})$,[14] which becomes

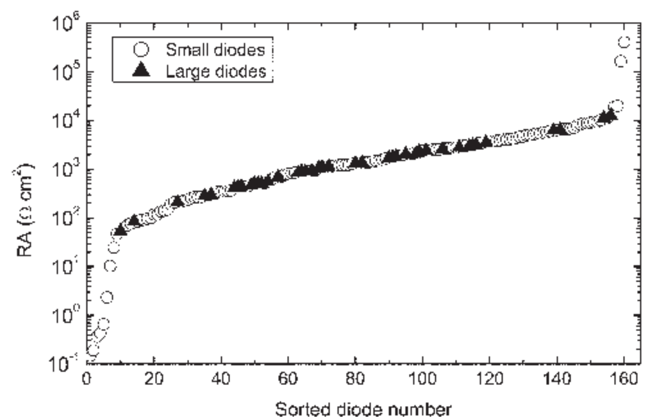

Fig. 5. Sorted R_0A values at 77 K for 120 16 × 16 μm² diodes and 40 37 × 37 μm² diodes from two 2-D arrays on the same sample with λ_{CO} = 5.3 μm (Sample 524–2). The measurements were made in the probe station.

Fig. 4. The 77 K image from the array of Fig. 3.

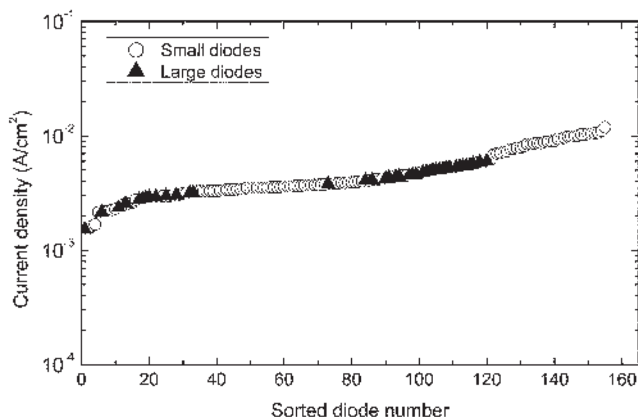

Fig. 6. Sorted $-I_0/A$ values for the same diodes as in Fig. 5. Five of the diodes with the lowest R_0A values in Fig. 5 had negative values of $-I_0/A$ and are not included in the plot.

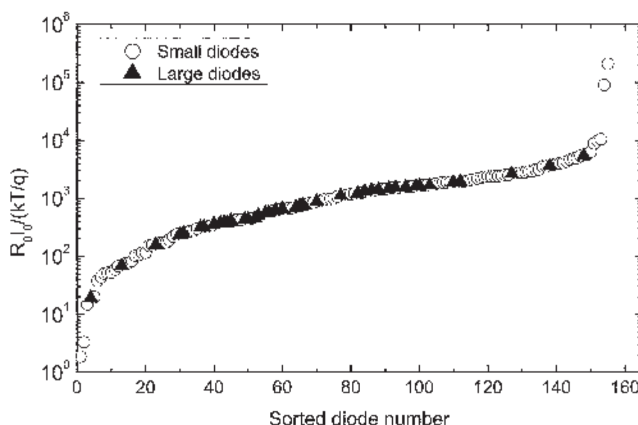

Fig. 7. Sorted $-I_0R_0$ values for the same diodes as in Fig. 5. Five of the diodes with the lowest R_0A values in Fig. 5 had negative values of $-I_0R_0$ and are not included in the plot.

$I_0R_0 >> kT/q$ for $I_{ph} = I_0$. Two of the diodes in Fig. 7 fall below this criterion, while the median values for I_0R_0 are 1190 kT/q for the small diodes and 677 kT/q for the large diodes. These test measurements were made in the probe station at 77 K.

On another sample from the same growth layer, 524-5, four 64 × 64 arrays were processed as described above and then In bumps were deposited on the diode areas. Unfortunately, the extra sample area outside the arrays was smaller than preferred, and many of the In bumps fell off in the process, especially around the edges of the four arrays. The sample was then cut into the individual arrays, and the best one was hybridized onto read-out electronics.

The arrays were characterized for uniformity, response, and noise. A set of 100 frames were recorded with a f/2 field of view at two temperatures differing by 10 K. The detector temperature was 77 K. The difference between the mean hot and cold outputs gave the responsivity at each pixel. The noise was obtained from the standard deviation of the 100 samples. The noise equivalent temperature difference was calculated from $NETD = (T_{hot} - T_{cold})(noise/responsivity)$.

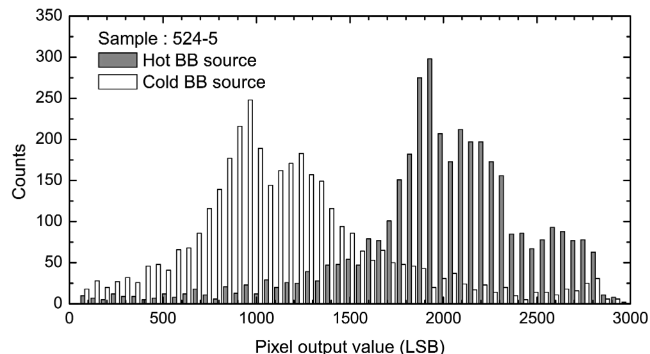

Fig. 8. Histogram of the pixel output values in a 64 × 64 element 2-D array with $\lambda_{CO} = 5.3$ μm for two blackbodies with a 10 K temperature difference. The units are LSB of the analog-to-digital converter. The sample is from the same growth layer as the one in Figs. 5–7.

Figure 8 shows a histogram of the pixel output values for the two blackbodies. Thirteen percent of the pixels gave output near zero and were counted as defective and are not included in the rest of the analysis. This number corresponds closely to an independent estimate from processing: approximately 10% of the In bumps were missing due to hybridization difficulties, mainly around the edges of the array. A histogram of the difference between the pixel output values at the two different temperatures, or responsivity, of the rest of the diodes is shown in Fig. 9. The average responsivity is 880 (median 950) with a standard deviation of 220 LSB (least significant bit of the analog-to-digital converter). Figure 10 shows the

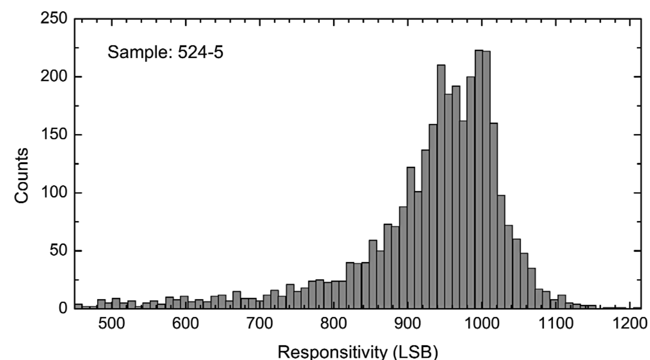

Fig. 9. Histogram of the responsivity for the nondefective pixels in the array of Fig. 8.

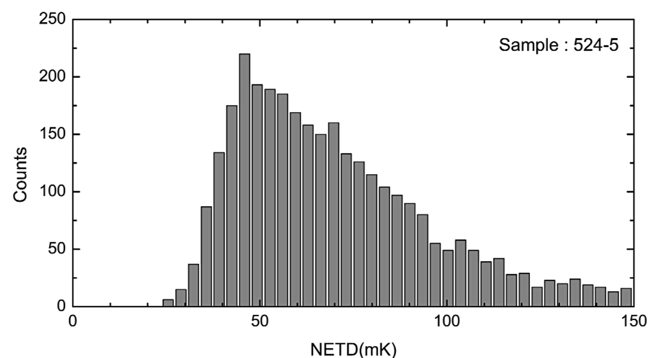

Fig. 10. NETD histogram of the values below 150 mK for the array in Fig. 8.

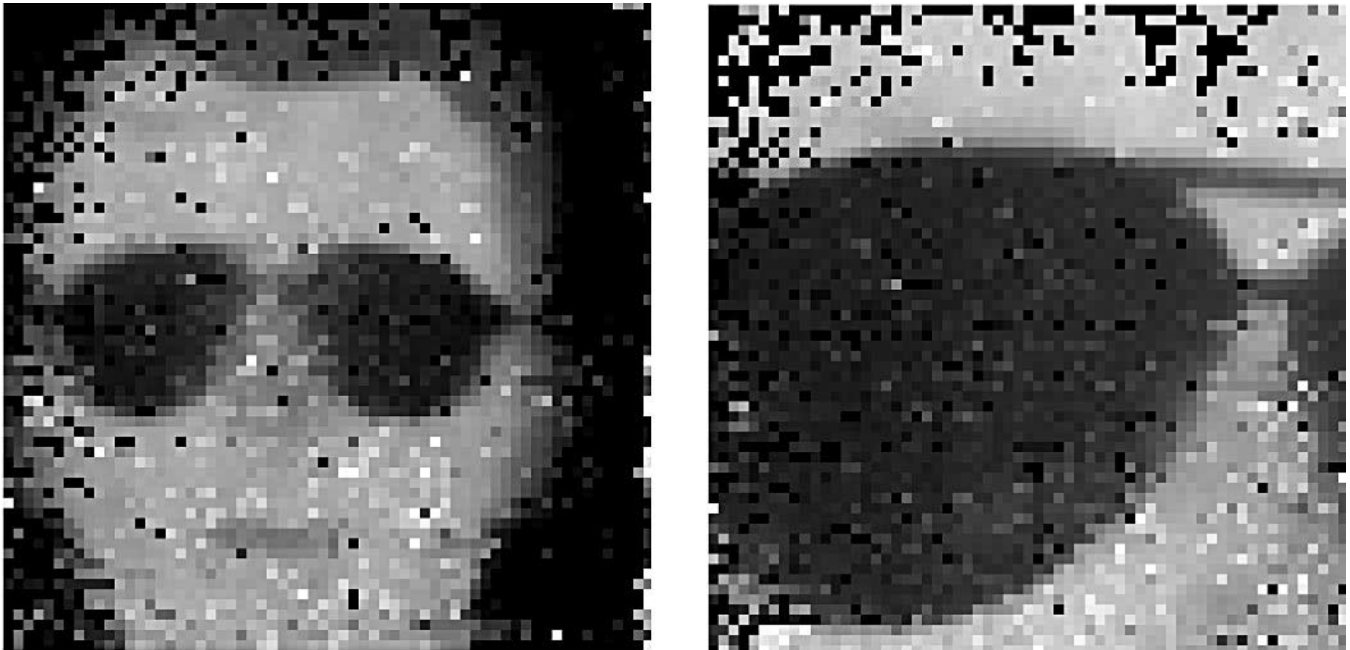

Fig. 11. Two 77 K images (without dead element correction) from the array of Fig. 8.

NETD histogram out to 150 mK. With a cutoff for operable diodes at 100 mK, 75% of the remaining diodes (after defective pixels, as defined above, are removed) are operable (this corresponds to 65% of the entire array), with a median value of 60 mK. With the cutoff at 150 mK, 88% of the nondefective diodes (76% of the entire array) are operable with a median of 65 mK. These values are higher than the theoretical background limited NETD of 13 mK for this system. This could possibly be due to low frequency noise in the diodes. Some images without dead element correction are shown in Fig. 11. The defective pixels are clearly seen mostly around the edges of the array.

SUMMARY

High-quality 1-D and 2-D arrays of planar photodiodes have been fabricated by ion milling of vacancy-doped MBE CMT layers on CZT. In-the-dark R_0A values at 77 K of 1.5–4 × 10^6 Ωcm^2 at cutoff wavelength λ_{CO} = 4.5 μm for four diodes in a 64-element linear array have been measured. Based on the uniformity and small leakage current of the probe station IV curves for all the diodes in the array, we believe that 61 of the 64 diodes have such high R_0A values. High quantum efficiency was also measured for the same growth layer. It was determined that a 0.5 μm CdTe passivation layer did not insulate properly between the p-type layer underneath and the Au lead-out wires on top, especially during ball bonding. A procedure including an extra ZnS passivation layer and electroplated Au on top of the sputtered bonding pads was developed, and it seems to prevent extra leakage current after bonding. Some 1-D arrays have been ball bonded to read-out electronics, and the best measured NETD on a LWIR array was 8 mK, with a median of 14 mK for the 42 operable diodes. The best measured NETD on a MWIR array was 18 mK. The 2-D arrays showed good uniformity of R_0A and I_0 values, and one 64 × 64 element array has been hybridized to read-out electronics. Approximately 10% of the In bumps fell off in the hybridization process. Of the rest of the diodes 75% had NETD below 100 mK, with median 60 mK, and 88% had NETD below 150 mK, with median 65 mK.

REFERENCES

1. K.D. Mynbaev and V.I. Ivanov-Omskii, *Semiconductors* 37, 1127 (2003).
2. M.V. Blackman, D.E. Charlton, M.D. Jenner, D.R. Purdy, and J.T.M. Wotherspoon, *Electron. Lett.* 23, 978 (1987).
3. E. Belas, P. Höschl, R. Grill, J. Franc, P. Moravec, K. Lischka, H. Sitter, and A. Toth, *Semicond. Sci. Technol.* 8, 1695 (1993).
4. R. Haakenaasen, T. Colin, H. Steen, and L. Trosdahl-Iversen, *J. Electron. Mater.* 29, 849 (2000).
5. R. Haakenaasen, T. Moen, T. Colin, H. Steen, and L. Trosdahl-Iversen, *J. Appl. Phys.* 91, 427 (2002).
6. K.D. Mynbaev and V.I. Ivanov-Omskii, *J. Alloy Compounds* 371, 153 (2004).
7. E. Belas, R. Grill, J. Franc, H. Sitter, P. Moravec, P. Höschl, and A.L. Toth, *J. Electron. Mater.* 31, 738 (2002).
8. R. Haakenaasen, H. Steen, T. Lorentzen, L. Trosdahl-Iversen, A.D. van Rheenen, and H. Syversen, *J. Electron. Mater.* 31, 710 (2002).
9. E. Belas, J. Franc, A. Toth, P. Moravec, R. Grill, H. Sitter, and P. Höschl, *Semicond. Sci. Technol.* 11, 1116 (1996).
10. J. Antoszewski, C.A. Musca, J.M. Dell, and L. Faraone, *J. Electron. Mater.* 32, 627 (2003).
11. T. Nguyen, C.A. Musca, J. M. Dell, J. Antoszewski, and L. Faraone, *J. Electron. Mater.* 32, 615 (2003).
12. T. Colin and T. Skauli, *J. Electron. Mater.* 26, 688 (1997).
13. M. Reine, *Infrared Detectors and Emitters: Materials and Devices,* ed. P. Capper and C.T. Elliott (Boston: Kluwer Academic Publishers, 2000), p. 341.
14. I.M. Baker, *Electronic Materials, Vol. 3: Narrow-gap II-VI Compounds for Optoelectronic and Electromagnetic Applications,* ed. P. Capper (London: Chapman and Hall, 1997), p. 452.